Journal of Materials Processing Tech. 305 (2022) 117576

Contents lists available at ScienceDirect

Journal of Materials Processing Tech.

journal homepage: www.elsevier.com/locate/jmatprotec

Solidification cracking of a nickel alloy during high-power keyhole mode laser welding

B. Mondal [a], M. Gao [b], T.A. Palmer [a,b], T. DebRoy [a,*]

[a] Department of Materials Science and Engineering, The Pennsylvania State University, University Park, PA, USA
[b] Department of Engineering Science and Mechanics, The Pennsylvania State University, University Park, PA, USA

ARTICLE INFO

Associate Editor: Dr Jian Cao

Keywords:
Laser welding
Keyhole mode welding
Solidification cracking
Nickel alloy
Modeling hot cracking

ABSTRACT

Nickel alloy Inconel 740H, a candidate material for use in ultra-supercritical power plants, is susceptible to solidification cracking during high power deep penetration laser welding. Here we examine how cracking is affected by welding variables and determine the locations where the cracks occur experimentally and theoretically. We use a solidification cracking model to calculate the effects of welding variables on cracking and the locations where the cracks form during high power laser keyhole mode welding of IN 740H. The parameters needed for the cracking model are obtained from a well-tested numerical heat transfer and fluid flow model for keyhole-mode welding. Model predictions of cracking and their locations for different welding conditions are verified by experiments.

1. Introduction

With growing environmental concerns of burning fossils fuels, coal-fired ultra-supercritical power plants operating at high steam temperatures around 760 °C and pressures about 35 MPa have been developed (Viswanathan et al., 2006). These operating conditions help to achieve high energy efficiency and low CO_2 emission rates (Tramošljika et al., 2021). These power plants require materials with superior creep and corrosion properties (Siefert et al., 2016). Inconel 740H, a precipitation-hardenable nickel alloy, is a candidate material for use in these plants because of its superior creep and corrosion resistance (Gianfrancesco, 2017). Kościelniak et al. (2021) showed that the microstructure of IN 740H was stable during its study of oxidation behavior in the steam atmosphere. However, fusion welds of IN 740H demonstrated reduced creep rupture life compared to the base material arising from the presence of γ' precipitate denuded zone (Bechetti et al., 2015). In another study, the mechanical properties of gas tungsten arc welds of 3.2 mm plates of IN 740H in a supercritical CO_2 atmosphere (Brittan et al., 2019) were found to be slightly impacted by the CO_2 atmosphere. The study of the susceptibility of the alloy to various types of cracking is also needed as a part of the material selection criteria. However, reports on cracking susceptibilities are available for a predecessor version of the alloy i.e. IN 740. Ramirez (2012) reported that IN 740 is highly susceptible to liquation cracking but not susceptible to ductility dip cracking. In a solidification cracking susceptibility study of several nickel alloys by Saito et al. (2019), IN 740 showed moderate susceptibility. The use of IN 740H in ultra-supercritical power plants will need the joining of thick plates. However, the cracking behavior of deep penetration welds of this alloy is not available in the literature.

Several investigations of solidification cracking of precipitation-hardenable Ni alloys have been reported in the literature. David et al. (2015) combined all recent efforts on welding and weldability of candidate Ni-based superalloys for advanced ultra-supercritical fossil power plants. Pakniat et al. (2016) compared weld penetration and the tendency of solidification crack in pulse laser welds of 2 mm thick Hastelloy X plates. Solidification cracking was found to decrease with an increase in pulse frequency and pulse duration. Wang et al. (2004) studied the effect of grain boundary misorientation on solidification cracking during welding of Ni-superalloy single and bi-crystals and showed that high grain boundary misorientation favors cracking. Solidification cracking in pulse laser welds of thin foils (0.2 mm thick) of IN 718 was reported by Lin et al. (2021) to propagate along Laves phase.

Solidification cracks form during the last stages of solidification when the mushy region experiences tensile stress, and the high solid fraction (fs>0.9) restricts the flow of liquid to backfill the cracks (Boellinghaus et al., 2016). Factors responsible for the solidification cracking include solidification temperature range, solidification parameters such as temperature gradient, solidification growth rate, and

* Corresponding author.
E-mail address: debroy@psu.edu (T. DebRoy).

https://doi.org/10.1016/j.jmatprotec.2022.117576
Received 15 November 2021; Received in revised form 21 March 2022; Accepted 27 March 2022
Available online 30 March 2022

Table 1
Thermophysical properties of IN 740H. These values were obtained from calculations using JmatPro for the alloy composition of IN 740 H. Here T represents the temperature in K and γ is the surface tension. The viscosity is at liquidus temperature.

Properties used for laser keyhole welding simulation	
Density (Kg/m^3)	8200
Dynamic viscosity (Kg/ms)	0.007
Solidus (K)	1425
Liquidus (K)	1669
Boiling point (K)	3063
Latent heat of fusion (J/Kg)	2.82×10^5
Specific heat (J/KgK)	$10^{-3}T^2 + 0.4T + 298$
Thermal conductivity (W/mK)	$0.013\ T + 9.177$
dγ/dT (N/mK)	-0.33×10^{-3}
Laser absorption coefficient	0.2
Laser power distribution	Gaussian
Laser radius (mm)	0.524
Laser power (W)	5000 – 10,000
Welding speed (mm/s)	12.7–38.1

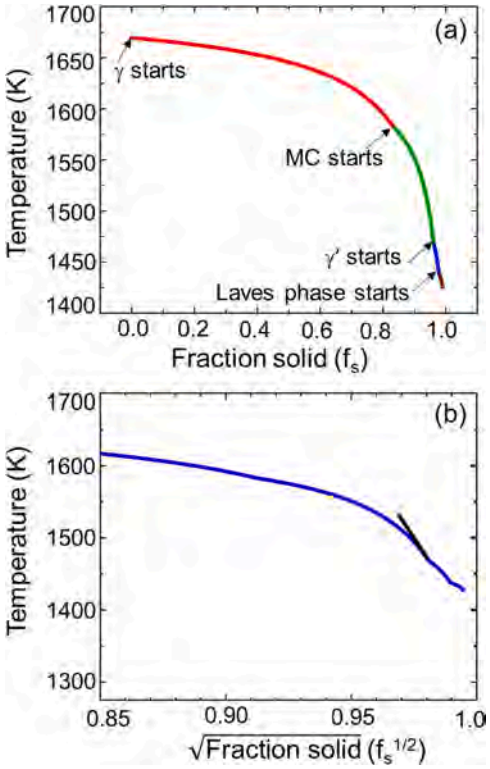

Fig. 1. (a) The temperature vs solid fraction (f_s) curve for IN 740H alloy calculated using ThermoCalc. (b) The maximum slope ($|dT/d(f_s)^{1/2}|$) of temperature versus $(f_s)^{1/2}$ curve (near $f_s = 0.96$) calculated using ThermoCalc where f_s is the mole fraction of solid is an important indicator of the susceptibility of an alloy to cracking.

cooling rate, and the amount of residual liquid during the last stages of solidification (Kou, 2020). The temperature gradient and the solidification growth rate influence the morphology of the solidification structure and lead to conditions that promote cracking susceptibility (Li et al., 2021).

Here we report the solidification cracking in laser keyhole mode welding of thick plates of IN 740H (12.7 mm) using high powers for several welding speeds. The origin of cracking is related to a cracking model that is based on the heat transfer and fluid model of the keyhole welding process. Additionally, the location of the cracks for each of the experimental welds is predicted from the cracking model.

Table 2
Comparison of experimentally observed crack depth and that predicted by using the model.

Laser power (kW)	Welding speed mm/s	Crack depth (Experiment) mm	Crack depth from crack susceptibility coefficient of 1.2
5	12.7	3.7–4.4	4.1
7.5	12.7	5–6.5	5.7
10	12.7	6.4–8	7.2
5	25.4	2.9–3.4	3.2
7.5	25.4	4.3–5.4	4.7
10	25.4	5.5–6.3	6.1
7.5	38.1	4–4.6	4.3
10	38.1	5.4 – 5.9	5.5

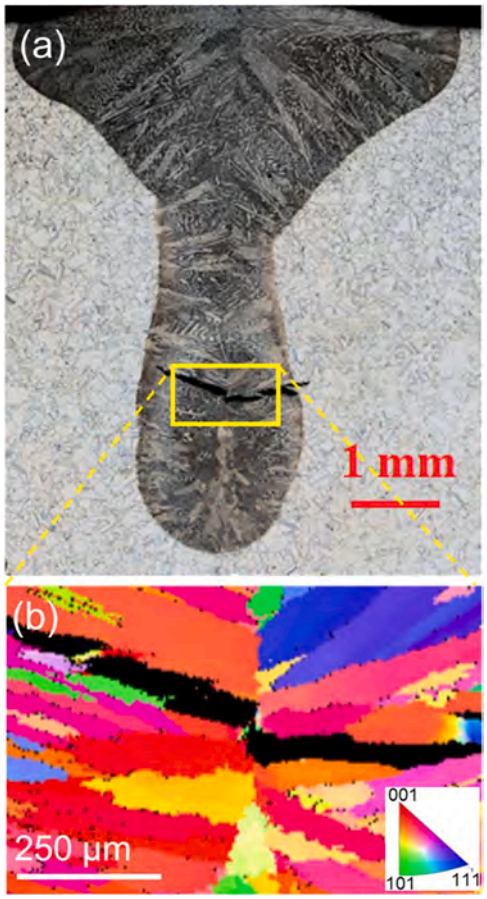

Fig. 2. (a) Representative etched optical cross-section image showing solidification crack in the keyhole region for a 5 kW weld and 12.7 mm/s welding speed on a 12.7 mm thick plate; (b) Inverse pole figure map of the region of crack (~depth of 5 mm) shows that it follows the grain boundary.

2. Materials and methods

2.1. Experimental welds

Keyhole mode welds were made on 12.7 mm thick plates of IN 740H using a laser radius of 0.524 mm. The laser power was varied between 5 kW and 10 kW and welding speeds of 12.7 mm/s, 25.4 mm/s, and 38.1 mm/s were used. The composition of the IN 740 H alloy plates used in this work (in wt%) is 50.07 Ni, 24.6 Cr, 20.3 Co, 0.2 Fe, 1.49 Nb, 0.05 Mo, 0.24 Mn, 1.4 Al, 1.5 Ti. 0.1 Si 0.03 C and 0.02 Cu.

Transverse cross-sections of all the welds were polished using standard metallographic techniques and observed in an optical microscope to identify the fusion zone size and shape. The locations of the cracks for

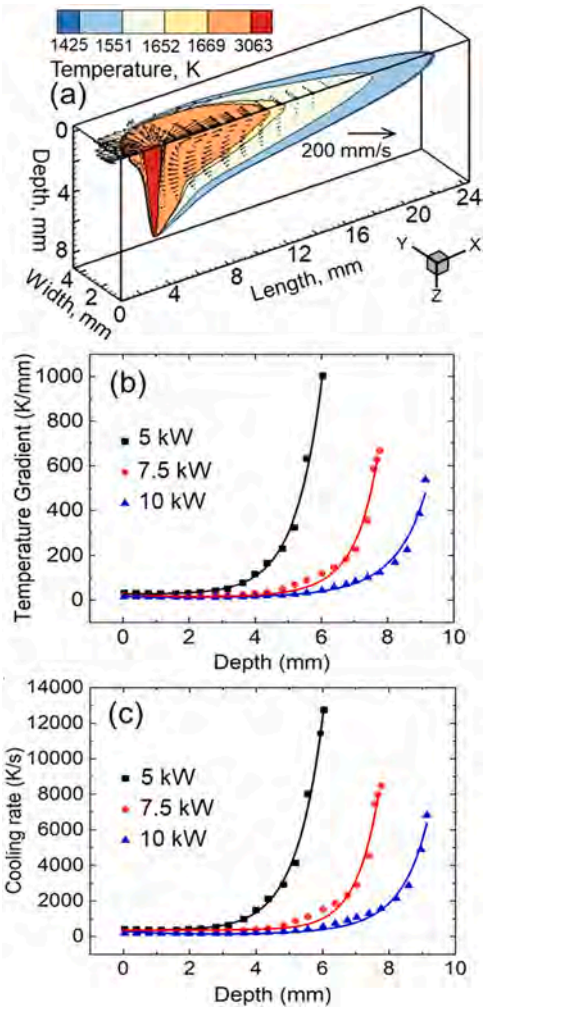

Fig. 3. (a) The calculated temperature and velocity fields during keyhole mode laser welding of IN 740H for 5 kW power and 12.7 mm/s welding speed. One-half of the pool is shown in a 3D isometric view due to symmetry across the vertical plane (XZ). The liquid metal flow is shown by the black velocity vectors and a reference vector is shown to estimate their magnitudes. Calculated temperature gradient (b) and cooling rate (c) in the mushy zone for different laser powers and 12.7 mm/s welding speed.

various laser powers and welding speeds were determined by scanning electron microscopy (with electron backscatter diffraction system) and 3D x-ray computed tomography (CT) scans. At least five measurements were made for determining the location of the depth of each crack for all the welding conditions.

2.2. Heat transfer and fluid flow model

We used a well-tested keyhole mode 3D heat transfer and fluid flow model to calculate the temperature fields, cooling rates, and the solidification behavior for various welding conditions. The details of the heat transfer and fluid flow model are available in our previous papers (Rai

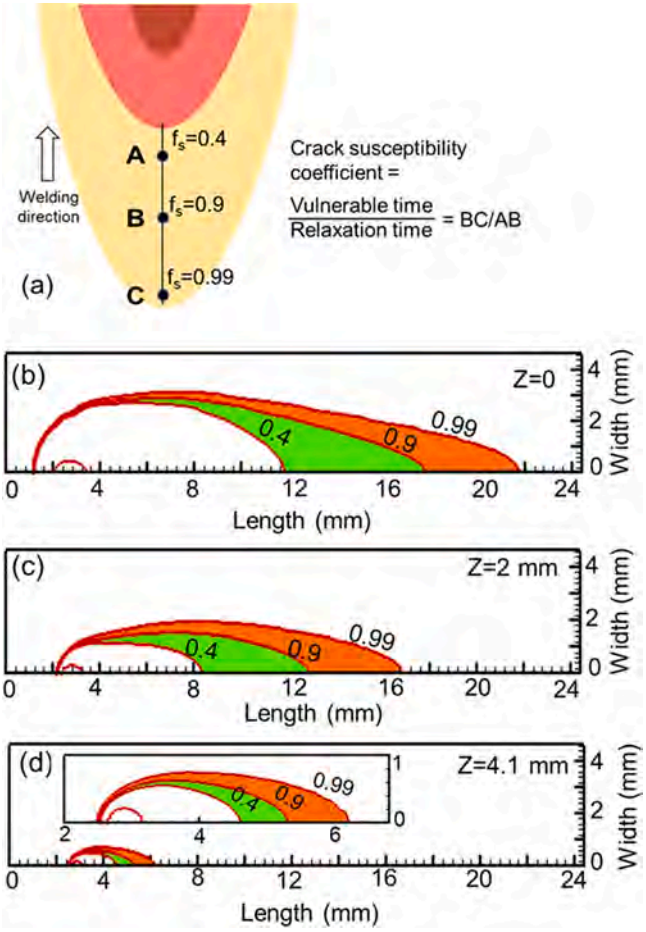

Fig. 5. (a) A schematic diagram showing the location of different solid fractions (f_s) in the mushy zone. The contours for solid fractions of 0.4, 0.9, and 0.99 for horizontal cross-sections (XY planes) with 5 kW at Z = 0 mm indicate contours at the top surface (Fig. b), the Z = 2 mm plane (Fig. c), and the Z = 4.1 mm plane (Fig. d).

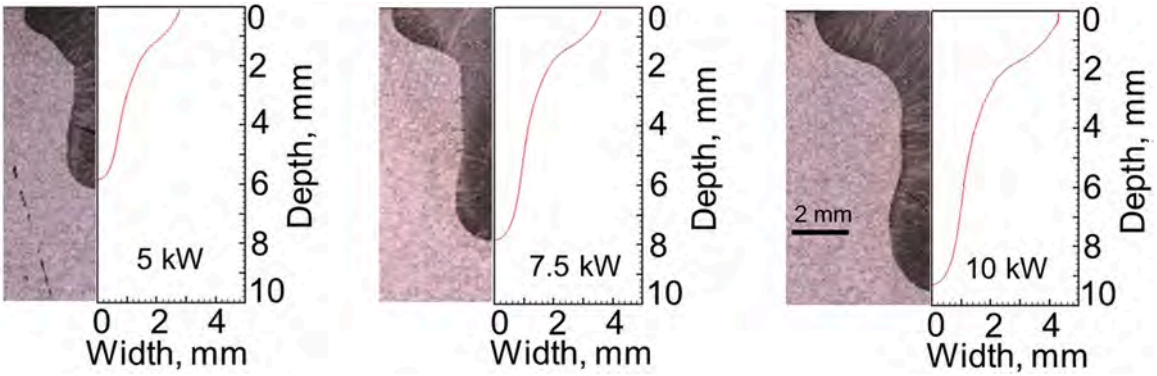

Fig. 4. Comparison of calculated and experimental weld geometry for different laser powers for a welding speed of 12.7 mm/s using 0.524 mm laser radius and 12.7 mm thick plate.

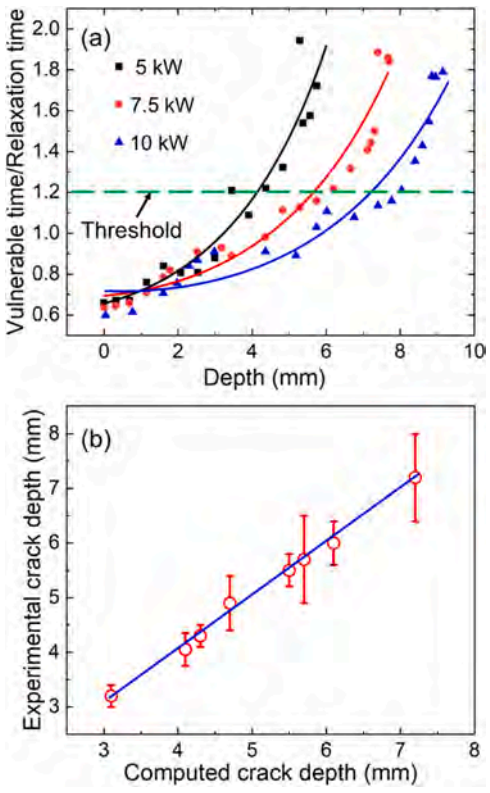

Fig. 6. (a) The calculated ratio of vulnerable time to relaxation time (cracking susceptibility coefficient) for different laser powers and 12.7 mm/s welding speed; (b) Relation between computed and experimental crack depth for different welding variables (Table 1).

et al., 2007a) and only the salient features are presented here. The calculation of the keyhole geometry is done first and then followed by heat transfer and fluid flow calculations (Rai et al., 2009). The calculation of the keyhole profile is done by a point by point heat balance at the keyhole wall which is at a temperature of the boiling point of the alloy (Rai et al., 2007b). The keyhole profile and the resulting heat flux are then used in a heat transfer and fluid flow model as a heat source and the equations of mass, momentum, and energy are solved for enthalpy and velocity. The 3D computed temperature fields are then used to calculate the solidification parameters. The thermophysical parameters of IN 740H used in the heat transfer and fluid flow model are extracted from JmatPro and are provided in Table 1.

3. Results and discussion

Solidification cracking has been associated with alloys having a large difference between the liquidus and solidus temperatures (Kou, 2020). A large solidification temperature range results in an expanded solid-liquid mushy zone volume, which shrinks considerably when cooled and increases the possibility of cracking. Calculations using the thermodynamic package ThermoCalc® show that Inconel 740H has a solidification temperature range of 244 K. The calculations show that solidification starts with the formation of primary γ followed by MC carbides, γ' precipitates, and finally terminates with the formation of Laves phase (Fig. 1a). The intermetallic Laves phase has an A2B general stoichiometry, where A elements (Ni, Cr, Fe) are smaller than the B elements (Nb, Mo, Ti) (Radhakrishna et al., 1995) Both γ' precipitates and the brittle Laves phase have been associated with solidification cracking in Ni alloys (Dupont et al., 2009). Sivaprasad and Raman (2008) conducted gas tungsten arc and electron beam welding on IN 718 and reported cracks to be prevalent adjacent to the Laves phase. Ye et al. (2015) reported that an increase in welding heat input increased the size of the Laves phase leading to increased weld metal solidification cracking susceptibility. Inconel 740H is characterized by both a large solidification temperature range and γ' precipitates which makes it susceptible to solidification cracking.

The relative susceptibility of solidification cracking has been successfully evaluated from temperature versus square root of fraction solid plots (Kou, 2015). A higher slope of the plot indicates a higher cracking susceptibility (Liu and Kou, 2017). For IN 740H, a plot of temperature versus square root of fraction solid calculated using ThermoCalc is shown in Fig. 1b. The plot has an increasing slope with decreasing temperature, and the steepest slope is observed when the solid fraction reaches about 0.96. This slope is higher than that for nickel alloy IN 718 which makes IN 740H more crack susceptible (Xia and Kou, 2020).

Our experiments showed cracks to be common in high-power keyhole mode laser welds of IN 740H. Table 2 shows the lowest and the highest depths where cracks were observed experimentally for various laser powers and welding speeds. A transverse cross-section of the weld for a 5 kW laser and 12.7 mm/s speed shows the characteristic wine glass shape of the fusion zone which is typical of the keyhole mode welding. A solidification crack is observed in the finger region of the fusion zone and extends beyond the fusion line boundary (Fig. 2a). Both horizontal and vertical orientations of the cracks were observed in several cross-sections of welds. The lowest and the highest depths of each crack were measured and the results are presented in Table 2. The intergranular nature of the solidification cracks in a deep penetration IN 740H weld is also evident from the inverse pole figure map shown in Fig. 2b. During welding of thick plates, the multi-axial stress states are transient and complex and the evolution of grain structure depends on welding parameters and the properties of the alloy. They are contributing factors to the geometry and orientation of cracks. In this investigation, cracks were observed in a plane normal to the plane of welding. Thus, the orientation of the cracks is different from that of the centerline cracks observed in some previous investigations. The reason for this difference is not known.

A quantitative investigation of solidification cracking in deep penetration keyhole mode welding requires knowledge of the temperature field, solid fraction distribution, and the fusion zone geometry for various welding variables. The cooling rates, temperature gradients, and the solidification growth rates affect the solidification microstructure (Blecher et al., 2014) which affects the cracking behavior. A computed weld pool geometry showing three-dimensional temperature and fluid flow patterns for IN 740H is shown in Fig. 3a. Model validations for several power levels and 12.7 mm/s welding speed is shown in Fig. 4. The high depth to width ratio of the keyhole weld is evident from this Fig. 3a. Heat transfer by conduction and convection in three dimensions affects the shape and size of the fusion zone. The keyhole geometry is indicated by the red-colored region enclosed by the boiling point of the alloy which is 3063 K. Liquid metal flows are indicated by black velocity vectors from the keyhole to the edge of the molten pool. The flow occurs because of the spatial gradient of surface tension which is stress known as the Marangoni stress. Since surface tension depends on temperature, the large spatial gradients of temperature at the weld pool surface result in large surface tension gradients which drive the flow. The mushy zone is bound by the liquidus temperature surface of 1669 K and the solidus temperature field of 1425 K. The weld pool and the mushy zone lengths decrease with increasing depth measured from the weld pool surface.

The scale and the morphology of the solidification microstructure are determined by the cooling rate and the ratio of the temperature gradient to the solidification growth rate, respectively. The computed values of the temperature gradients in the mushy zone along the welding direction as a function of depth are shown in Fig. 3b. They are calculated by dividing the difference between the liquidus and solidus temperatures by the length of the mushy zone at various depths and represent the temperature gradient at 1547 K. The computed values of the temperature gradients change from 32 to 1003 K/mm for a weld made using 5 kW laser power and 12.7 mm/s welding speed. Multiplying the

temperature gradient by the welding speed provides the cooling rate at each depth measured from the surface of the welds. The results are presented in Fig. 3c. The computed results show that the cooling rate increases from 405 K/s at the weld surface to 12,741 K/s at a depth of about 6 mm, which is the bottom of the keyhole for 5 kW laser power and 12.7 mm/s welding speed. Higher cooling rates have been associated with the formation of cracks (Chelladurai et al., 2015). Our experimental data show that for all power and speed combinations, cracks occurred in the keyhole region at various depths but not at the bottom of the keyhole (Table 1). Since both the temperature gradient and the cooling rate increase continuously with depth, they cannot be directly used to determine the location of the cracks within the weldments.

Clyne and Davies (1981) proposed a hot cracking susceptibility coefficient, which is the ratio of the duration when the solid-liquid two--phase region is vulnerable to cracking and the relaxation time available for the stress relief process. The vulnerable time is defined in their model (Clyne et al., 1982) as the time needed for the solid-liquid mixture to solidify from the solid fraction of 0.9–0.99. During this period, the liquid metal available in the two-phase solid-liquid mixture is thought to be insufficient to fill up and compensate for the shrinkage of the last liquid as the two-phase mixture cools. On the other hand, the relaxation time is defined by the progression of solidification during changes in the solid fraction from 0.4 to 0.9. During this time, the solidification shrinkage can be easily backfilled because of the availability of a large volume of liquid. The procedure for the calculation of the hot cracking susceptibility coefficient is illustrated in Fig. 5a. A high value of the coefficient indicates a greater time of exposure of the two-phase mixture to vulnerable conditions indicating a greater likelihood of cracking. As illustrated in Fig. 5a, specific locations where the solid fractions are 0.4, 0.9, and 0.99 within the two-phase region in the molten pool are needed to use the hot cracking model. They are calculated from the three-dimensional temperature field which depends on the welding variables such as laser power and welding speed. Furthermore, the cracking susceptibility coefficient can be calculated at different depths of welds. Such calculations will enable an evaluation of the values of the hot cracking susceptibility coefficient at locations where the cracks are found within the weldments from experiments for different conditions of welding. The relation between temperature and the solid fraction is obtained from the Scheil curve calculated from the thermodynamic package ThermoCalc. The calculations show that temperatures of 1425 K, 1551 K, 1652 K, and 1669 K corresponded to solid fractions of 0.99, 0.9, 0.4, and 0, respectively. The solid fractions contours at three depths are shown in Fig. 5b, Fig. 5c and Fig. 5d. They show the green regions bound by solid fractions between 0.4 and 0.9, which represent the relaxation region and the red regions bound by solid fractions of 0.9 and 0.99, which represent the vulnerable region at three depths.

We consider several XY horizontal cross-sections which represent various weld depths to examine the changes in the lengths of vulnerable and relaxation regions and the corresponding hot cracking susceptibility coefficients. The weld pool and the mushy zone lengths decrease with increasing depth from the pool surface. The coefficients calculated for 5, 7.5, and 10 kW laser powers and 12.7 mm/s welding speed shows that for each power, the ratio of the vulnerable time to relaxation time increases continuously with depth as shown in Fig. 6a. Furthermore, the depths corresponding to the vulnerable time to the relaxation time of 1.2 matches the depths where cracks are observed experimentally in each case. Fig. 6b shows a plot of the location of the cracks observed experimentally to the depth at which the ratio of the vulnerable time to relaxation time has a ratio of 1.2. The agreement shows that for the deep penetration keyhole mode laser welding of alloy 740H, the crack depth observed experimentally agrees with that calculated theoretically for a ratio of vulnerable time to relaxation time ratio of 1.2. When this threshold is crossed, i.e., when the value of the crack susceptibility coefficient is higher than 1.2, no other cracks have been observed experimentally.

As we have seen in Fig. 6a, the computed values of the crack susceptibility coefficient increase with depth. Why then are no other cracks observed at higher depths? It seems that once the value of the coefficient reaches 1.2, a higher value of the coefficient does not nucleate new cracks, but rather propagates the existing crack. What is most important is that this threshold value of the ratio holds for all powers and speeds investigated in this work and it allows identification of the depth where the cracks appear in each case. This analysis of the threshold can also help to avoid cracking by changing the laser power and welding speed. Increasing laser power (at constant welding speed) while providing greater depth of weld penetration also shifts the crack to greater depths (Fig. 6a).

Summary and conclusions

In summary, we present experimental data and theoretical calculations to examine the cracking behavior of high power, keyhole mode laser welding of Inconel 740H. We related the welding variables with the occurrence of cracks and their locations using a cracking susceptibility model. The necessary values of vulnerable time and relaxation time were obtained from a well-tested keyhole mode heat transfer and fluid flow model. The model predictions were compared with the experimental results. The following are the main findings.

(a) Inconel 740H suffers from solidification cracking during thick section keyhole mode laser welding at laser powers of 5 kW, 7.5 kW, and 10 kW and 12.7, 25.4, and 38.1 mm/s welding speeds. This behavior is consistent with the large solidification temperature range of this alloy of 244 K.
(b) Increasing power at a constant welding speed increases the pool volume. Thus the two-phase mushy zone volume, enclosed between isotherms of 1425 K and 1669 K, also increases.
(c) At a constant welding speed, the cracks occurred at greater depths with the increase in laser power from 5 kW to 10 kW. At constant laser powers, the cracks occurred at lower depths with increasing welding speed.
(d) The cracking susceptibility model could predict the locations of cracks using computed values of the cracking susceptibility coefficient of 1.2 for all values of laser powers and welding speeds investigated.

Declaration of Competing Interest

The authors declare that they have no known competing financial interests or personal relationships that could have appeared to influence the work reported in this paper.

Acknowledgments

The Inconel 740H plate material used in the welding experiments was provided by Dr. T.M. Lillo at the Idaho National laboratory. Dr. Lillo also provided many helpful discussions that contributed to the analysis. We also thank Dr. J.S. Zuback for his help with the Scheil calculations of IN 740H. Computations for this research were performed on the Pennsylvania State University's Institute for Computational and Data Sciences' Roar supercomputer. This manuscript has in part been authored by Battelle Energy Alliance, LLC under Contract No. DE-AC07–05ID14517 with the U.S. Department of Energy under Award Number FWP-B100–19010. The United States Government retains and the publisher, by accepting the paper for publication, acknowledges that the United States Government retains a nonexclusive, paid-up, irrevocable, worldwide license to publish or reproduce the published form of this manuscript, or allow others to do so, for United States Government purposes.

CRediT authorship contribution statement

B Mondal: Conceptualization, Formal analysis, Investigations, Data curation, Software, Writing – original draft, review & editing. **M Gao**: Investigations. **T A Palmer**: Conceptualization, Supervision, Writing – review & editing. **T DebRoy**: Conceptualization, Methodology, Supervision, Writing – review and editing.

Appendix A. Calculation of the ratio of the vulnerable time to relaxation time

The temperature field in the mushy zone is obtained from the heat transfer and fluid model. Each temperature in the mushy region represents a specific solid fraction. The Scheil plot of IN 740H (Fig. 1) shows that 1652 K, 1551 K, and 1425 K correspond to solid fractions of 0.4, 0.9, and 0.99, respectively. The following figure shows the top view of a molten pool at the top surface (Z = 0). The green region of the mushy zone shows solid fractions between 0.4 and 0.9 and the red region shows solid fractions between 0.9 and 0.99.

The length of the vulnerable region (BC) = 3.967 mm.

The length of the relaxation region (AB) = 6.011 mm.

The times spent in these regions are obtained by dividing the zone lengths by the welding speed (12.7 mm/s). Thus, the time spent in the vulnerable region is (3.97/12.7) s and the time spent in the relaxation region is (6.01/12.7) s. The cracking susceptibility coefficient is the ratio of time spent in the vulnerable region to that in the relaxation region. Its value is the ratio of lengths BC and AB and is obtained as 3.97/6.01 = 0.66.

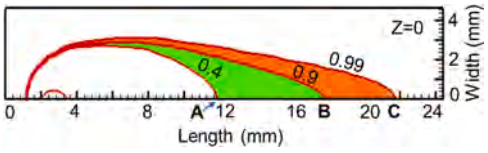

Fig. A1. A schematic diagram showing lines of various solid fractions on a top plane of a weld.

References

Bechetti, D.H., DuPont, J.N., Barbadillo, J.J.D., Baker, B.A., Watanabe, M., 2015. Microstructural evolution of INCONEL alloy 740H fusion welds during creep. Metall. Mater. Trans. A. 46, 739–755.

Blecher, J., Palmer, T.A., DebRoy, T., 2014. Solidification map of a nickel-base alloy. Metall. Mater. Trans. A 45, 2142–2151.

Boellinghaus, T., Lippold, J.C., Cross, C.E. (Eds.), 2016. Cracking Phenomena in Welds IV. Springer International Publishing, Switzerland.

Brittan, A.M., Mahaffey, J., Anderson, Mark, Sridharan, K., 2019. Effect of supercritical CO2 on the performance of 740H fusion welds. Mater. Sci. Eng. A 742, 414–422.

Chelladurai, A.M., Gopal, K.A., Murugan, S., Albert, S.K., Venugopal, S., Jayakumar, T., 2015. Effect of energy transfer modes on solidification cracking in pulsed laser welding. Sci. Technol. Weld. Join. 20, 578–584.

Clyne, T.W., Davies, G.J., 1981. The influence of composition on solidification cracking susceptibility in binary alloy systems. Br. Foundrym. 74, 65–73.

Clyne, T.W., Wolf, M., Kurz, W., 1982. The Effect of melt composition on solidification cracking of steel, with particular reference to continuous casting. Metal. Trans. B 13, 259–266.

David, S.A., Siefert, J.A., DuPont, J.N., Shingledecker, J.P., 2015. Weldability and weld performance of candidate nickel base superalloys for advanced ultrasupercritical fossil power plants part I:fundamentals. Sci. Technol. Weld. Join. 20, 532–552.

Dupont, J.N., Lippold, J.C., Kiser, S.D., 2009. Welding Metallurgy and Weldability of Nickel-base Alloys, first ed. John Wiley & Sons Inc, New Jersey.

Gianfrancesco, A.D., 2017. Materials for Ultra-Supercritical and Advanced Supercritical Power Plants, first ed. Woodhead Publishing, Amsterdam.

Kościelniak, B., Chmiela, B., Sozańska, M., Swadźba, R., Drajewicz, M., 2021. Oxidation behavior of inconel 740H nickel superalloy in steam atmosphere at 750 °C. Materials 14, 4536.

Kou, S., 2015. A criterion for cracking during solidification. Acta Mater. 88, 366–374.

Kou, S., 2020. Welding Metallurgy, third ed. John Wiley & Sons Inc, New Jersey.

Li, Y., Li, H., Katgerman, L., Du, Q., Zhang, J., Zhuang, L., 2021. Recent advances in hot tearing during casting of aluminium alloys. Prog. Mater. Sci. 117, 100741.

Lin, J., Wang, X., Lei, Y., Wei, R., Guo, F., 2021. Study on hot cracking in laser welded joints of inconel 718 alloy foils. J. Manuf. Process. 64, 1024–1035.

Liu, J., Kou, S., 2017. Susceptibility of ternary aluminum alloys to cracking during solidification. Acta Mater. 125, 513–523.

Pakniat, M.F., Ghaini, M., Torkamany, M.J., 2016. Hot cracking in laser welding of Hastelloy X with pulsed Nd:YAG and continuous wave fiber lasers. Mater. Des. 106, 177–183.

Radhakrishna, C.H., Prasad Rao, K., Srinivas, S., 1995. Laves phase in superalloy 718 weld metals. J. Mater. Sci. Lett. 14, 1810–1812.

Rai, R., Roy, G.G., DebRoy, T., 2007a. A computationally efficient model of convective heat transfer and solidification characteristics during keyhole mode laser welding. J. Appl. Phys. 101, 054909.

Rai, R., Elmer, J.W., Palmer, T.A., DebRoy, T., 2007b. Heat transfer and fluid flow during keyhole mode laser welding of tantalum, Ti–6Al–4V, 304L stainless steel and vanadium. J. Phys. D: Appl. Phys. 40, 5753–5766.

Rai, R., Burgardt, P., Milewski, J.O., Lienert, T.J., DebRoy, T., 2009. Heat transfer and fluid flow during electron beam welding of 21Cr–6Ni–9Mn steel and Ti–6Al–4V alloy. J. Phys. D: Appl. Phys. 42, 025503.

Ramirez, J.E., 2012. Susceptibility of IN740 to HAZ liquation cracking and ductility-dip cracking. Weld. J. 91, 122s–133s.

Saito, N., Komai, N., Hashimoto, K., Kitamura, M., 2019. Evaluation of weld cracking susceptibility of candidate ni-based alloys for advanced usc boilers. In: Shingledecker, J., Takeyama, M. (Eds.), Joint EPRI-123HiMAT International conference on Advances in High Temperature Materials. ASM International, Nagasaki, Japan, pp. 1048–1059.

Siefert, J.A., Shingledecker, J.P., DuPont, J.N., David, S.A., 2016. Weldability and weld performance of candidate nickel based superalloys for advanced ultrasupercritical fossil power plants. Sci. Technol. Weld. Join. 21, 397–427.

Sivaprasad, K., Raman, S.G.S., 2008. Influence of weld cooling rate on microstructure and mechanical properties of alloy 718 weldments. Metall. Mater. Trans. A 39, 2115–2127.

Tramošljika, B., Blecich, P., Bonefačić, I., Glažar, V., 2021. Advanced ultra-supercritical coal-fired power plant with post-combustion carbon capture: analysis of electricity penalty and CO_2 emission reduction. Sustainability 13, 801.

Viswanathan, R., Coleman, K., Rao, U., 2006. Materials for ultra-supercritical coal-fired power plant boilers. Int. J. Press. Vessel. Pip. 83, 778–783.

Wang, N., Mokadem, S., Rappaz, M., Kurz, W., 2004. Solidification cracking of superalloy single- and bi-crystals. Acta Mater. 52, 3173–3182.

Xia, C., Kou, S., 2020. Evaluating susceptibility of Ni-base alloys to solidification cracking by transverse-motion weldability test. Sci. Technol. Weld. Join. 25, 690–697.

Ye, X., Hua, X., Wang, M., Lou, S., 2015. Controlling hot cracking in Ni-based Inconel-718 superalloy castsheets during tungsten inert gas welding. J. Mater. Process. Technol. 222, 381–390.